Cryptococcus neoformans Rim101 Is Associated with Cell Wall Remodeling and Evasion of the Host Immune Responses

Teresa R. O'Meara,[1,3] Stephanie M. Holmer,[2] Kyla Selvig,[1,3] Fred Dietrich,[3] and J. Andrew Alspaugh[1,3]

Departments of Medicine,[1] Cell Biology,[2] and Molecular Genetics and Microbiology,[3] Duke University School of Medicine, Durham, North Carolina, USA

ABSTRACT **Infectious microorganisms often play a role in modulating the immune responses of their infected hosts. We demonstrate that *Cryptococcus neoformans* signals through the Rim101 transcription factor to regulate cell wall composition and the host-pathogen interface. In the absence of Rim101, *C. neoformans* exhibits an altered cell surface in response to host signals, generating an excessive and ineffective immune response that results in accelerated host death. This host immune response to the *rim101*Δ mutant strain is characterized by increased neutrophil influx into the infected lungs and an altered pattern of host cytokine expression compared to the response to wild-type cryptococcal infection. To identify genes associated with the observed phenotypes, we performed whole-genome RNA sequencing experiments under capsule-inducing conditions. We defined the downstream regulon of the Rim101 transcription factor and determined potential cell wall processes involved in the capsule attachment defects and altered mechanisms of virulence in the *rim101*Δ mutant. The cell wall generates structural stability for the cell and allows the attachment of surface molecules such as capsule polysaccharides. In turn, the capsule provides an effective mask for the immunogenic cell wall, shielding it from recognition by the host immune system.**

IMPORTANCE ***Cryptococcus neoformans* is an opportunistic human pathogen that is a significant cause of death in immunocompromised individuals. There are two major causes of death due to this pathogen: meningitis due to uncontrolled fungal proliferation in the brain in the face of a weakened immune system and immune reconstitution inflammatory syndrome characterized by an overactive immune response to subclinical levels of the pathogen. In this study, we examined how *C. neoformans* uses the conserved Rim101 transcription factor to specifically remodel the host-pathogen interface, thus regulating the host immune response. These studies explored the complex ways in which successful microbial pathogens induce phenotypes that ensure their own survival while simultaneously controlling the nature and degree of the associated host response.**

Received 12 November 2012 **Accepted** 6 December 2012 **Published** 15 January 2013

Citation O'Meara TR, Holmer SM, Selvig K, Dietrich F, Alspaugh JA. 2013. *Cryptococcus neoformans* Rim101 is associated with cell wall remodeling and evasion of the host immune responses. mBio 4(1):e00522-12. doi:10.1128/mBio.00522-12.

Editor Liise-anne Pirofski, Albert Einstein College of Medicine

Address correspondence to Andrew Alspaugh, andrew.alspaugh@duke.edu.

Disease due to the opportunistic fungus *Cryptococcus neoformans* is increasingly important in the face of the expanding HIV/AIDS epidemic and the use of immunosuppressant drugs. Over 600,000 deaths per year can be attributed to cryptococcosis; the majority of these infections occur in patients with AIDS in resource-limited countries (1). *C. neoformans* is also an excellent model to study the interaction of a eukaryotic pathogen with its infected host.

Outcomes of infections are dependent on complex interactions between the vigor of the host immune response and the intrinsic virulence of the pathogen. Therefore, recent studies of microbial pathogenesis have explored the importance of the immune response to infection as a mediator of host damage in addition to examining direct microbial injury of the host. While many microbial pathogens express toxins or other virulence factors that directly damage the host, overactivation of the host immune system can similarly cause host damage, such as when immunogenic superantigens result in bacterial toxic shock syndromes (2). Cryptococcal disease can also be understood within this damage-response framework. In the face of severe host immunodeficiency, pathogens such as *C. neoformans* induce host damage and symptomatic disease primarily by microbial proliferation. In fact, one of the primary predictors of a poor host outcome of cryptococcal meningitis is a very low number of inflammatory cells present in the cerebrospinal fluid (CSF) at the time of infection (3). However, in other patients, restoration of a dysfunctional immune system can cause immune hyperactivation against subclinical cryptococcal infections, resulting in progressive symptoms despite effective microbial killing. This immune reconstitution inflammatory syndrome (IRIS) emphasizes the potential role of the host immune system in mediating host damage and disease symptoms (4).

One of the classic markers of *C. neoformans* adaptation to the host is the induction of a polysaccharide capsule. The dominant paradigm is that acapsular *C. neoformans* strains either fail to cause disease or are severely attenuated in disease progression. This has been demonstrated for multiple acapsular strains, including an early series of capsule mutants (*cap59*Δ, *cap60*Δ, *cap64*Δ), and in other unencapsulated variants (5–8). Concordantly, hypercapsular strains can be hypervirulent in the host (9, 10).

Previous work demonstrated multiple roles for the capsule in

virulence modulation. One role is the prevention of phagocytosis by macrophages, an important environmental niche inside the host (11). Glucuronoxylomannan (GXM), the primary capsule component, can alter phagocytosis rates (12, 13). After phagocytosis, the capsule may defend against reactive oxygen species produced by macrophages (14). The capsule also has a direct role in suppressing the immune system by titrating out complement components and preventing a more active inflammatory response (15, 16). We propose that the capsule also acts as a barrier against immune recognition of cell wall components such as α-glucan, β-glucan, chitin/chitosan, and mannans. These conserved fungal cell wall components can act as potent pathogen-associated molecular patterns (PAMPs), triggering a highly active immune response (17–19). Thus, the capsule may play multiple roles in the modulation of host immune responses. The cell-shielding effect of the capsule on pathogenesis was previously difficult to examine because of the intrinsically poor virulence of capsule-deficient strains. Therefore, the capsule-deficient but infection-competent *rim101*Δ mutant strain offers unique insight into the interaction of host cells and the exposed *C. neoformans* cell wall (20).

Recently, we and others demonstrated the paradoxical observation that the hypocapsular *rim101*Δ mutant strain was hypervirulent in two animal models of cryptococcosis (20, 21), revealing a discordance between *C. neoformans* capsule defects and the expected subsequent reductions in virulence. To further examine the relationships among Rim101, the capsule, and virulence, we examined the inflammatory response to *rim101*Δ mutants, the downstream Rim101 targets, and the roles of these targets in virulence. In this paper, we demonstrate that a pulmonary infection with the *rim101*Δ mutant strain results in a fundamentally different disease progression characterized by excessive activation of the host inflammatory system. We suggest a model in which the absence of Rim101 leads to an inability of this fungus to appropriately remodel the cell wall, which has functional consequences for capsule attachment and exposure of previously shielded PAMPs. Additionally, Rim101 controls cellular responses to variations in environmental pH, thus regulating proliferation within macrophages.

Our results demonstrate how *C. neoformans* has adapted conserved transcription factors, such as Rim101, to control fundamental cellular processes that allow its survival in the host. Our results also suggest new models defining the interplay of molecules on the surface of pathogens that can control the level of host immune activation, thus leading to pathogen control, dormancy, or host damage.

RESULTS

Infection with the *rim101*Δ mutant strain results in increased host inflammation. To define the role of Rim101 in pathogenesis, we performed detailed studies of fungal survival *in vivo* and the resulting host immune response. We previously tested the *rim101*Δ mutant strain in an inhalation model of murine cryptococcosis using the A/J mouse strain, which has a defect in complement activation (20). To ensure that this observation was not dependent on the mouse background, we infected female C57BL/6 mice (10 per strain) by intranasal inoculation with 2×10^4 CFU of the wild-type (WT), *rim101*Δ mutant, or acapsular *cap59*Δ mutant strain. Mice were monitored for survival and sacrificed at predetermined clinical endpoints predicting death (Fig. 1A). Infection of C57BL/6 mice with either the *rim101*Δ mutant or WT strain resulted in similar death kinetics, with no significant difference in animal survival between the strains ($P = 0.67$).

Even though the absolute death rates of the two groups were similar, mice infected with the *rim101*Δ mutant strain demonstrated strikingly different symptoms of disease. Mice infected with WT *C. neoformans* typically develop prominent neurological symptoms immediately prior to exhibiting profound weight loss, predicting imminent death. In contrast, the *rim101*Δ mutant-infected mice developed predominant respiratory symptoms (rapid and labored breathing) prior to weight loss and death. This differential pattern of symptomatic disease progression was similar in both mouse strains. As expected, all mice infected with the acapsular *cap59*Δ mutant strain cleared the infection without any disease symptoms and survived for the duration of the experiment (Fig. 1A) (5).

To examine host responses to the *rim101*Δ mutant strain, we performed histological analyses of infected lungs at various time points after infection in both the A/J (Fig. 1B) and C57BL/6 (see Fig. S1A in the supplemental material) mouse backgrounds. Images of the reconstituted strain are presented in Fig. S1B. In A/J mice infected with the WT strain, there were numerous fungal cells with large capsular haloes present throughout the lung tissue at both 4 and 14 days after infection. The underlying alveolar architecture of the lung parenchyma was clearly visualized, with limited foci of leukocytes associated with encapsulated yeast cells, often adjacent to blood vessels. The inflammatory cells were composed primarily of mononuclear cells, with rare eosinophils and neutrophils (Fig. 1C).

Mouse lungs infected with the *rim101*Δ mutant demonstrated a very different histological pattern at both 4 and 14 days after infection. Even at the early time point, the lung tissue was filled with an intense inflammatory cell infiltrate (Fig. 1B). By day 14, the inflammatory cell infiltrate completely obscured the alveolar spaces, consistent with the clinical symptoms of respiratory distress observed in these animals (Fig. 1B). In the *rim101*Δ mutant-infected lungs, the inflammatory cells consisted predominantly of neutrophils and eosinophils. Small yeast cells with thin capsular haloes were observed amid the host inflammatory infiltrate (Fig. 1C).

To ensure that the altered pattern of inflammation in the *rim101*Δ mutant-infected mice was not due to an increased fungal burden, we performed quantitative cultures of tissues from these infections. We first cultured bronchoalveolar lavage fluid obtained from infected mice after 2 and 4 days of infection (Fig. 1D). At both time points, we observed significantly more WT cells than *rim101*Δ mutant cells (day 2, 3.8×10^4 CFU/ml [WT] versus 0.6×10^4 CFU/ml [*rim101*Δ mutant] [$P < 0.01$]; day 4, 8.4×10^5 CFU/ml [WT] versus 1.7×10^5 CFU/ml [*rim101*Δ mutant] [$P < 0.0001$]). Using whole-lung homogenization at day 9, we similarly observed a 4.9-fold greater fungal burden in the WT than in the mutant strain ($P < 0.0106$). Therefore, the increased inflammatory response cannot be attributed to an increased number of *rim101*Δ mutant cells within the infected lungs.

We also noted a striking difference in fungal morphology *in vivo* between the WT and *rim101*Δ mutant strains. WT cells displayed a marked range of sizes, from small budding yeast cells (approximately 5 μm) to large and highly encapsulated titan cells (15 to 50 μm), a newly described *C. neoformans* morphotype characterized by enlarged cells with extensive and tightly linked capsules (22, 23). In contrast, the *rim101*Δ mutant displayed small

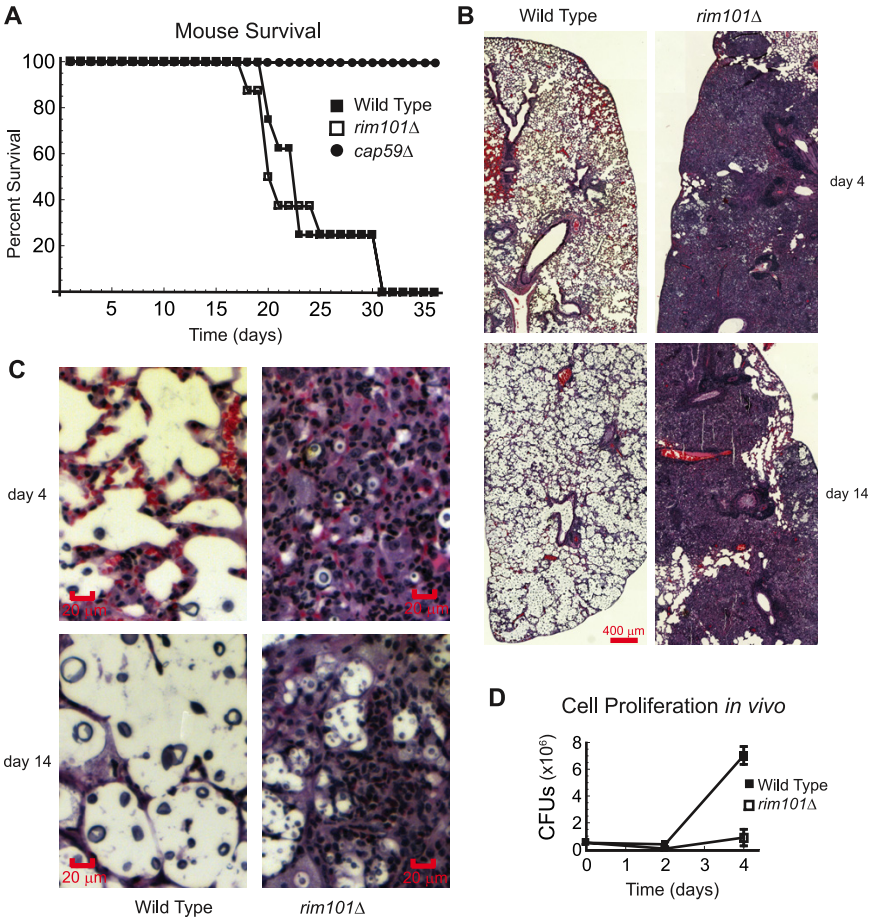

FIG 1 Effects of Rim101 on *C. neoformans* virulence, immune cell infiltration, and inflammation. (A) Hypocapsular *rim101*Δ mutant cells maintain virulence in a murine model of cryptococcosis. C57BL/6 mice (10 per strain) were inoculated intranasally with 2×10^4 cryptococcal cells and monitored for survival. (B) Histopathologic analysis demonstrated increased inflammation in *rim101*Δ mutant-infected mice. A/J mouse lungs were harvested on days 4 and 14 postinfection, and the infected lungs were assessed by histopathologic analysis. (C) Histopathologic analysis demonstrated increased influx of PMN cells into *rim101*Δ mutant-infected mice. A/J mouse lungs were harvested on days 4 and 14 postinfection, and the infected lungs were assessed by histopathologic analysis. (D) The virulence of the *rim101*Δ mutant is not due to the fungal burden. Lavage fluid was collected from five mice per strain on days 2 and 4 to quantify fungal burdens and cell proliferation *in vivo*.

and minimally encapsulated fungal cells *in vivo*, with limited size variation. To quantify this difference in cell size, we directly measured the diameters of 500 cells of each strain recovered by bronchoalveolar lavage on day 4. The WT strain exhibited a broad range of cell sizes, with 33.6% titan cells (defined as cells >15 μm in diameter [22]). In contrast, most of the *rim101*Δ mutant cells were present as small yeast cells, with few titan cells (2.0%), consistent with prior data linking Rim101 and titan cell formation (24) (Fig. 2A). Overall, the average diameter of the *rim101*Δ mutant cells was significantly smaller than that of non-titan WT cells (WT, 13.9 ± 6.24 μm; *rim101*Δ mutant, 6.75 ± 2.76 μm [$P < 0.0001$]). When cell were incubated *in vitro*, their size did not differ between the strains, even after incubation under tissue culture conditions (WT, 6.3 ± 1.3 μm; *rim101*Δ mutant, 6.2 ± 1.0 μm [$P = 0.27$]). Despite their smaller size, the *rim101*Δ mutant cells were equally as viable as WT cells, as assessed by the comparative germination rates of visualized cells within the lung lavage fluid (data not shown).

Although titan cells have a noted defect in the ability to cross the blood-brain barrier (22), the variation in size between the WT and *rim101*Δ mutant cells appeared to have no effect on dissemination from the lungs, with both WT and *rim101*Δ mutant cells showing equivalent numbers of CFU in the spleen on day 4, consistent with our previous work showing similar fungal burdens by quantitative culture of the brains on days 9 and 14 (20). Therefore, we hypothesize that the altered virulence of the *rim101*Δ mutant strain is not due to increased dissemination.

Titan cells have also been recently implicated in the regulation of inflammation during cryptococcal lung infections. An increase in the proportion of titan cells is associated with decreases in the phagocytosis of cryptococcal cells and in overall inflammation (23, 25). To test whether the *rim101*Δ mutant phenotype can be attributed primarily to a lack of titan cells, we coinfected the lungs with both strains to provide a source of titan cells. A/J mice were infected intranasally with a total of 2×10^4 cryptococcal cells with a 1:1, 2:1, or 1:2 ratio of WT to *rim101*Δ mutant cells. After day 4, the lungs were harvested and analyzed via histopathologic analysis (Fig. 2B). We observed that coinfected lungs had more inflammation than lungs infected with just the WT strain, despite abundant (a minimum of 19.2%) titan cells (Fig. 2B). The amount of inflammation correlated most closely with the initial dose of *rim101*Δ mutant cells; however, we observed inflammation even in areas containing both titan cells and smaller *rim101*Δ mutant cells, suggesting that titan cells cannot completely protect against *rim101*Δ mutant-driven inflammation (Fig. 2C).

Altered cytokine and cellular immune responses to the *rim101*Δ mutant. To better quantify the population of inflammatory cells in the mouse lung after infection with 5×10^5 WT or *rim101*Δ mutant cells, we collected bronchoalveolar lavage fluid from A/J mice for cytokine and leukocyte analysis 4 days after infection. We performed cytospin analysis of the lavage fluid and used hematoxylin and eosin (H&E) staining to differentiate the various cell populations by morphology, as described previously (26). As is apparent from the histopathologic analysis of lung sections, total lung leukocytes were greatly increased in *rim101*Δ mutant-infected mice (Fig. 1B and C). Moreover, the vast majority of these inflammatory cells were neutrophils (Fig. 3A). Mice infected with the *rim101*Δ mutant strain showed a statistically significantly higher percentage of neutrophils and eosinophils than mice infected with the WT strain or the saline control (Fig. 3A; see Table S1 in the supplemental material). As expected, we did not observe a significant influx of lymphocytes at this early

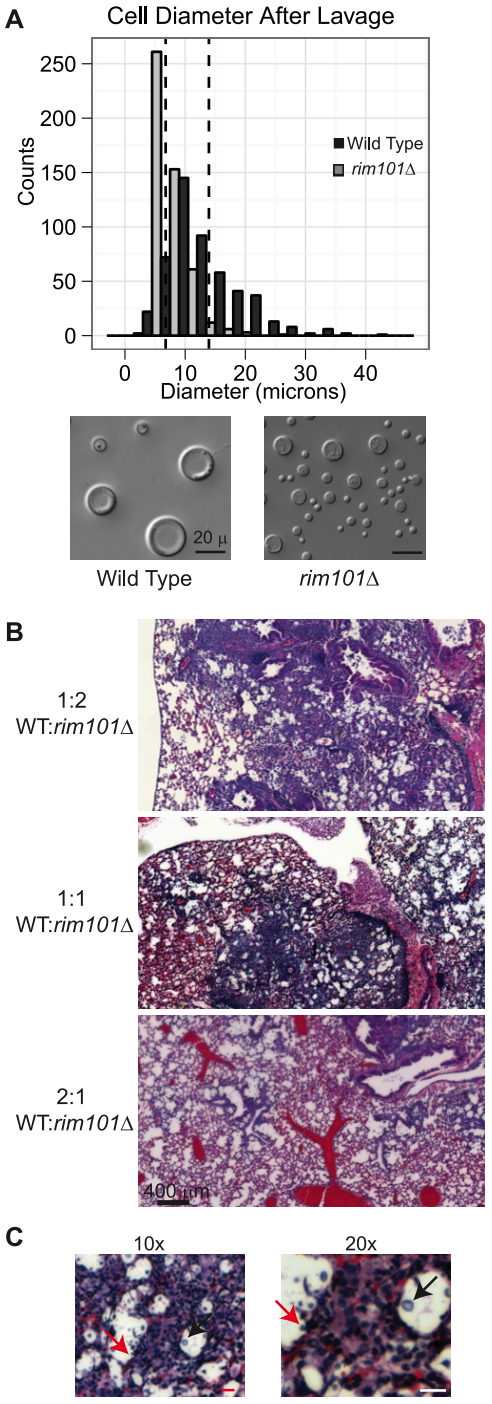

FIG 2 Rim101 regulates *C. neoformans* cell size *in vivo*. (A) *rim101*Δ mutant cells are smaller than WT cells *in vivo*. Fungal cells were harvested from mouse lungs by lavage at 4 days postinfection and examined microscopically. Diameters were measured by using ImageJ. (B) Coinfected lungs demonstrate *rim101*Δ mutant-mediated inflammation. Mice were infected with the indicated ratios of WT to *rim101*Δ mutant cells for a total of 5×10^5 cells per mouse. Lungs were harvested on day 4 postinfection and subjected to histopathologic analysis. (C) Titan cells are not sufficient to prevent *rim101*Δ mutant-mediated inflammation. Mice were infected with equal numbers of WT and *rim101*Δ mutant cells for a total of 5×10^5 cells per mouse. Lungs were harvested at day 4 postinfection and subjected to histopathologic analysis. Local foci of inflammation contain both titan cells and smaller *rim101*Δ mutant cells. Arrows indicate the two cell size populations present in each lung.

time point, consistent with a predominantly innate immune response.

We also examined the levels of 20 murine cytokines from the lavage fluid by using Luminex multiplex assays. Overall, we saw higher cytokine levels in mice infected with the *rim101*Δ mutant strain than in WT-infected mice and phosphate-buffered saline (PBS)-treated controls. In accordance with previous studies, we did not observe significant differences between the cytokine profiles of WT-infected and PBS-treated mouse lungs at this time point, suggesting that the WT is effective at damping or avoiding the host immune response (27, 28). Of particular note were the levels of interleukin-12 (IL-12), gamma interferon (IFN-γ)-inducible protein 10 (IP-10)/CXCL10, MIG/CXCL9, MIP1-α, VEGF (vascular endothelial growth factor), and tumor necrosis factor alpha (TNF-α), all of which were significantly higher in *rim101*Δ mutant-infected mice (Fig. 3B; see Table S2 in the supplemental material). Many of these are proinflammatory cytokines that have previously been implicated in the accumulation of immune cells, clearance of *C. neoformans* from the lung, and eventual Th1 weighting of the adaptive immune response (29).

Rim101 is involved in cell wall remodeling under host-relevant conditions. The exuberant innate response observed early in *rim101*Δ mutant infection suggested that the *rim101*Δ mutant cells were aberrantly exposing an antigenic trigger. In other fungi, Rim101 regulates cell wall remodeling in response to specific environmental stimuli. For example, CaRim101 directs the *Candida albicans* yeast-hyphal transition in response to alkaline pH (30–32). Therefore, we hypothesized that the Rim101 protein in *C. neoformans* is also involved in the regulation of the cell wall structure when activated by host environmental signals.

To test this hypothesis, we examined WT and *rim101*Δ mutant cells by transmission electron microscopy (TEM) after incubation either under tissue culture conditions (Dulbecco's modified Eagle's medium [DMEM] with 5% CO_2 at 37°C) or in rich medium (yeast extract-peptone-dextrose [YPD]). Under rich growth conditions, there was no significant difference in cell wall thickness between the strains (WT, 152.76 nm; *rim101*Δ mutant, 136.6 nm [$P = 0.44$]). However, under tissue culture conditions, *rim101*Δ mutant cells had extremely thick cell walls compared to those of the WT (WT, 139.11 nm; *rim101*Δ mutant, 445.08 nm [$P < 0.001$]) (Fig. 4A).

Rim101 transcriptionally regulates cell wall genes. To determine the genes associated with the cell wall changes observed in the *rim101*Δ mutant strain, we performed comparative transcriptional profiling. We sequenced total RNA extracted from either the WT or *rim101*Δ mutant strain after induction in DMEM for 3 h at 37°C with 5% CO_2. A subset of the Rim101-regulated genes from this data set has been previously published (24).

The Rim101 transcription factor controls the expression of a large number of genes directly or indirectly, with 1,257 genes displaying an at least 2-fold transcript level differential between WT and *rim101*Δ mutant cells (see Table S3 in the supplemental material). Among these, we found many genes involved in cell wall biosynthesis, maintenance, and remodeling (Table 1). In the *C. neoformans* genome, there are 12 genes with an identified role in the synthesis of chitin and chitosan, the predominant components of the cell wall. Eight of these genes were differentially expressed by the WT and *rim101*Δ mutant strain, suggesting that Rim101 regulates their expression under host conditions. Additionally,

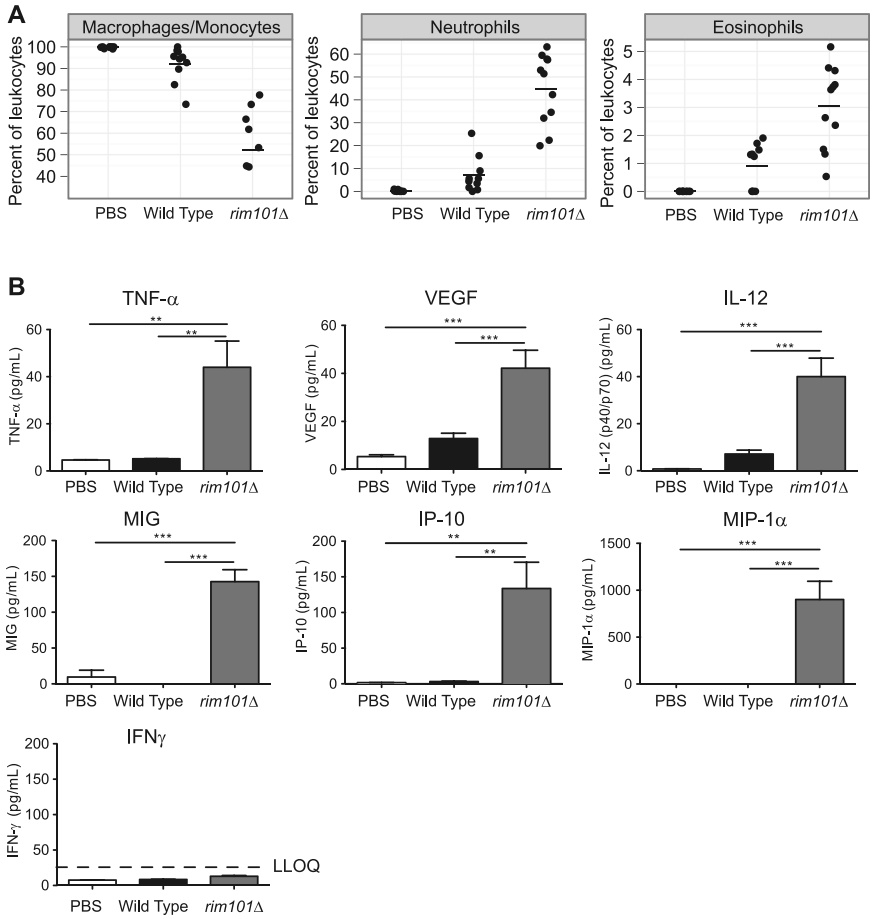

FIG 3 Rim101 mediates innate immune cell responses. (A) *rim101*Δ mutant-mediated infection is characterized by PMN cell influx. Lavage fluid for cytospin analysis was collected from mice that had been infected with the WT ($n = 10$) or the *rim101*Δ mutant ($n = 11$) or treated with a PBS control ($n = 10$). Slides were stained with H&E, and the cells were characterized and quantified on the basis of morphological characteristics. Bars indicate means ± the standard errors of the means. (B) *rim101*Δ mutant cells induce increased cytokine responses. Lavage fluid was collected from mice infected with the WT ($n = 10$) or the *rim101*Δ mutant ($n = 11$) or treated with a PBS control ($n = 10$). Cytokine levels were assessed by multiplex ELISA. Data represent means ± the standard errors of the means for four independent experiments, each with at least three mice per group. Statistical significance was determined by one-way ANOVA with Bonferroni correction. **, $P < 0.01$; ***, $P < 0.001$; LLOQ, lower limit of quantification.

Rim101-regulated gene expression is reflected in altered cell wall composition. To assess the altered composition of the *rim101*Δ mutant cell wall and the functional effects of Rim101-mediated cell wall gene expression, we examined α-(1,3)-glucan, chitin/chitosan, and β-glucan levels in the *rim101*Δ mutant and WT strains. Using a biochemical assay for cell wall chitin/chitosan content (34), we confirmed 1.45-fold higher levels of these cell wall polymers in the *rim101*Δ mutant strain than in the WT ($P < 0.05$). We confirmed these results and monitored the dynamic changes in cell wall chitin/chitosan content using fluorescein isothiocyanate (FITC)-conjugated wheat germ agglutinin (WGA) to stain the oligomeric form of chitin. When either the WT or *rim101*Δ mutant strain was incubated in rich medium, we observed fluorescence at only the bud necks, consistent with previous observations of localized chitin deposition at this site (35, 36). We observed increased chitin staining in both the WT and *rim101*Δ mutant strains after 2 h of incubation in tissue culture medium, manifesting as an increasing percentage of cells with diffuse fluorescence/chitin incorporation throughout the cell wall (Fig. 4B). In the WT cells, the percentage of cells with this enhanced pattern of chitin deposition decreased quickly during an 8-h time course, with the majority of the cells demonstrating chitin localization only at the bud neck by the end of the observation period (Fig. 4B). In contrast, the *rim101*Δ mutant strain maintained a high percentage of cells with elevated chitin staining, even after 8 h (Fig. 4B).

We also examined the role of Rim101 in α-glucan localization and abundance. This cell wall molecule is required for virulence in the fungal pathogen *Histoplasma capsulatum* because it prevents host recognition of immunogenic components in the cell wall (37). In *C. neoformans*, α-glucan is the only known cell wall component required for capsule attachment. Using a labeled antibody against α-glucan (37), we determined that WT cells show a gradual, time-dependent increase in the levels of this cell wall component during incubation under tissue culture conditions, consistent with an increasing average capsule diameter around these cells (Fig. 4C). We observed similar patterns of increased α-glucan incorporation into the cell walls of the *rim101*Δ mutant cells, although more of the *rim101*Δ mutant than WT strain cells stained for α-(1,3)-glucan after 8 h of induction (Fig. 4C). Because neither strain exhibited α-glucan staining after incubation in rich medium, we hypothesize that α-glucan is specifically induced by *C. neoformans* in response to host environmental cues.

Finally, we stained cells with aniline blue to examine β-(1,3)-

five of these genes contain a putative Rim101 binding site in the 1,000 bp upstream of the start codon (20, 33), consistent with direct Rim101 activation, as opposed to the altered *rim101*Δ mutant cell wall merely resulting as a nonspecific response to cell stress. Genes encoding other major elements of fungal cell walls were also differentially transcribed in a Rim101-dependent manner, including the β-glucan synthase genes *FKS1*, *SKN1*, and *KRE6* and the α-glucan synthase gene *AGS1*.

To examine the regulation of some of these genes, we performed targeted reverse transcription (RT)-PCR experiments with candidate cell wall genes after the cells had been incubated in either rich medium or tissue culture medium for 3 h (see Table S4 in the supplemental material). We were able to recapitulate the overall pattern of gene expression changes observed via RNA-Seq. For a few genes, we observed divergent regulation under rich medium and tissue culture conditions (*CDA3*, *KRE6*, *CHI22*), although in some cases, the overall *n*-fold changes were minimal.

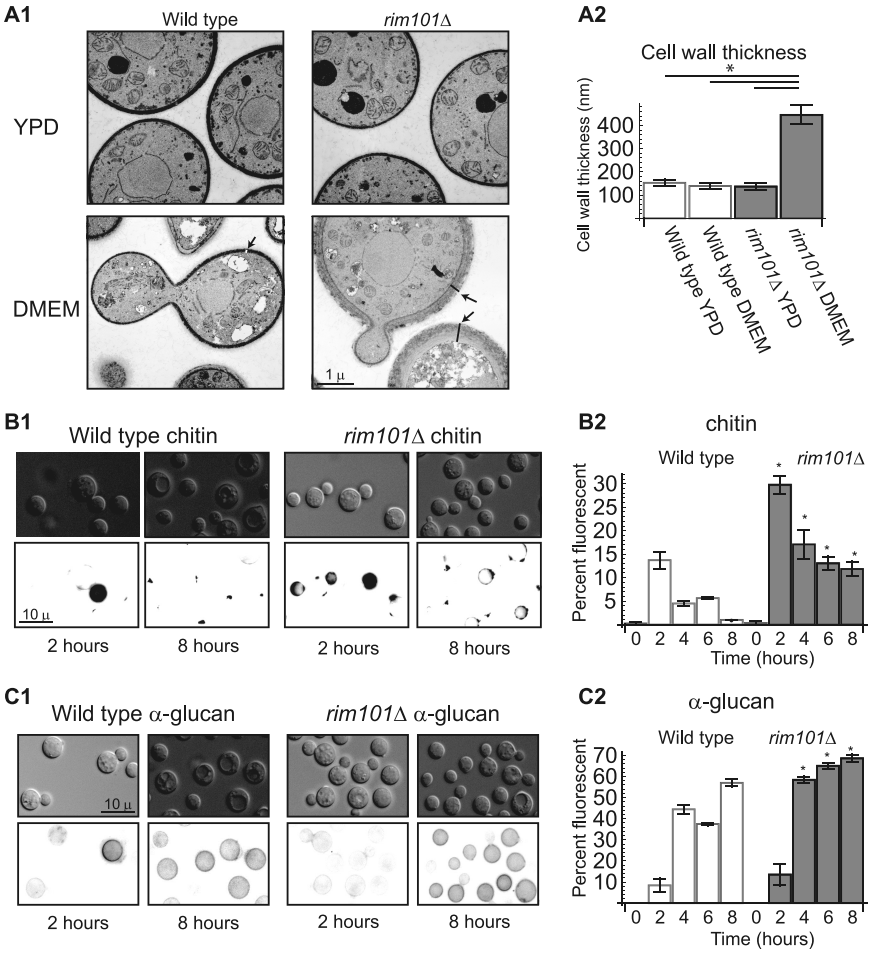

FIG 4 Rim101 regulates cell wall components. (A1, A2) *rim101*Δ mutant cell walls are significantly thicker than those of the WT under inducing conditions. (A1) TEM was performed after incubation in either YPD or DMEM (capsule-inducing conditions). Arrows on the TEM micrographs indicate representative cell wall measurements. (A2) ImageJ was used to quantify cell wall thickness. Values are means ± the standard errors of the means. Two-way ANOVA with Bonferroni correction was used to determine statistical significance (*, $P < 0.001$). (B1, B2) *rim101*Δ mutant cells have increased chitin/chitosan under inducing conditions. Cells were stained with FITC-conjugated WGA after induction in CO_2-independent medium at 37°C. The percentage of cells demonstrating fluorescence around the entire cell was determined. (B1) Representative fluorescence patterns at the indicated time points. (B2) Quantification of the fluorescence patterns using ImageJ analysis of multiple microscopic fields. (C1, C2) *rim101*Δ mutant cells have increased α-glucan under inducing conditions compared to the WT level. (C1) Cells were incubated with the MOPC-104E antibody and the fluorescent anti-IgM secondary antibody after induction in CO_2-independent medium at 37°C. The percentages of cells demonstrating fluorescence around the entire cell were determined. Representative fluorescence patterns at the indicated time points. (C2) Quantification of the fluorescence patterns using ImageJ analysis of multiple microscopic fields.

glucan levels after induction in DMEM or YPD (38). Under both conditions, WT and *rim101*Δ mutant cells showed similar patterns of cell surface fluorescence (data not shown). Together, these results indicate that Rim101 controls multiple cell wall synthesis proteins under host-relevant conditions. However, the main physiological effect of Rim101 on the cell wall appears to be the control of chitin/chitosan and α-glucan content.

Altered cell walls affect capsule attachment and phagocytosis. *C. neoformans* capsule induction has three major stages: biosynthesis within the cell, secretion through the cell wall, and attachment and maintenance at the cell surface. Previously, we demonstrated that the *rim101*Δ mutant strain was able to synthesize and secrete capsular material despite its defect in surface capsule expression (20). We therefore hypothesized that *rim101*Δ mutant-mediated changes in cell wall composition would have functional consequences for capsule attachment, providing the mechanism of the hypocapsular phenotype of the *rim101*Δ mutant. To better differentiate which of these processes is dependent on Rim101, we first tested the ability of secreted polysaccharides from WT and *rim101*Δ mutant cells to bind to the cryptococcal cell surface. Previous work demonstrated that capsule-deficient strains, such as the *cap59*Δ mutant strain, are able to passively bind exogenous polysaccharide from encapsulated strains (39). We used this strain as a recipient of passive capsule binding to assess the function of secreted capsular material from the WT and *rim101*Δ mutant strains by using indirect immunofluorescence with an anticapsular antibody (monoclonal antibody [MAb] 18b7). Secreted polysaccharides from conditioned medium from either *rim101*Δ mutant or WT cells were able to passively bind to *cap59*Δ mutant cells, restoring the surface capsule to this acapsular strain. Moreover, the patterns of surface fluorescence were similar between the strains (Fig. 5A). When we cocultured *cap59*Δ mutant cells with *cap59*Δ mutant-conditioned medium, we observed no surface capsule staining, as expected for a strain with a known defect in polysaccharide secretion (40, 41). These results are most consistent with a model in which the *rim101*Δ mutant capsule defect is due to its altered cell wall and aberrant capsule binding rather than intrinsic alterations in polysaccharide synthesis or structure.

Given its intact capsule synthesis and defective capsule binding, we hypothesized that the *rim101*Δ mutant would shed more polysaccharide into the medium than would the WT strain. We quantified the exopolysaccharide levels by using an established protocol of electrophoresis and immunoblotting of conditioned medium from the WT and *rim101*Δ mutant strains, using a series of 2-fold dilutions to quantify the relative levels of shed GXM (Fig. 5B). This analysis revealed that the *rim101*Δ mutant strain releases approximately four times as much GXM into the medium as the WT strain does. The WT strain retains significantly more capsule at the cell surface, thus maintaining a more substantial barrier between the fungal cell and the host immune system.

To further examine the potential physiological consequences of altered surface capsule on phagocytosis, we assessed the effects of Rim101-dependent cell wall changes on phagocytosis rates. In

TABLE 1 Differentially regulated cell wall genes between WT and *rim101*Δ mutant strains

Genomic ID	Annotation	*n*-Fold change (WT/*rim101*Δ mutant)
CNAG_00546	Chitin synthase 6	−2.86
CNAG_00897	*SKN1* β-(1,6)-glucan synthase protein	10.08
CNAG_00914	*KRE6* β-glucan synthesis protein	−2.68
CNAG_01234	Spore wall assembly-related protein	−3.55
CNAG_01239	*CDA3* chitin deacetylase	−8.83
CNAG_02298	Glucan 1,4-α-glucosidase, putative	−3.13
CNAG_02850	*AGN1* glucan endo-1,3-α-glucosidase	−2.18
CNAG_02860	Endo-1,3(4)-β-glucanase, putative	2.39
CNAG_03120	*AGS1* α-glucan synthase protein	−2.05
CNAG_04033	α-Glucosidase	−2.61
CNAG_04245	Chitinase *CHI22*	−6.36
CNAG_05581	Chitin synthase 4	−2.69
CNAG_05663	*SCW1* cell wall integrity protein	−5.84
CNAG_05799	*CDA1* chitin deacetylase	4.78
CNAG_05818	*CHS5* chitin synthase	−2.44
CNAG_06508	*FKS1* β-(1,3)-glucan synthase	−5.31
CNAG_06835	*KRE61* β-(1,6)-glucan synthesis protein	8.26
CNAG_07499	Chitin synthase 8	−2.70

our previous work, we determined that there was no difference in phagocytosis between the WT and *rim101*Δ mutant strains (20). In contrast, recent work by Chun et al. showed that *rim101*Δ mutant cells have a higher rate of association with macrophage cells than WT cells do after 24 h of coincubation (42). However, both of these prior experiments were performed under conditions that would not induce capsule or cell wall changes in cryptococcal cells. Therefore, we compared the phagocytosis of WT and *rim101*Δ mutant cells after incubation in either rich medium (noninducing conditions) or tissue culture medium (inducing conditions) for 12 h (Fig. 5C).

Both induced and uninduced cells were opsonized with mAb 18b7 before coincubation with phorbol myristate acetate (PMA)-activated J774A.1 macrophages in standard phagocytosis assays (20). After 2 h, unengulfed cryptococcal cells were removed by gentle washing. The macrophages were then lysed and plated for CFU counting. As expected, induction of capsule around the WT cells caused a 1.28-fold decrease in the phagocytosis rate (87.7 versus 68.1%; $P < 0.004$). Induction under tissue-mimicking conditions caused a 1.24-fold decrease in phagocytosis in *rim101*Δ mutant cells (88.1 versus 71.0%; $P < 0.02$). Under both conditions, there was no significant difference in phagocytosis between the *rim101*Δ mutant strain and the WT strain.

Finally, to examine the role of shed polysaccharide in these interactions, we preincubated *cap59*Δ mutant cells with conditioned medium from either the WT or the *rim101*Δ mutant strain for 1 h before examining phagocytosis. Compared with untreated cells, there was no statistically significant difference in the phagocytosis rates of *cap59*Δ mutant cells coated with either WT or *rim101*Δ mutant strain-shed polysaccharide (87.23 versus 91.07%; $P = 0.12$), suggesting that the capsular material shed by either strain minimally affects cryptococcal cellular phagocytosis in this assay (Fig. 5).

Rim101 induces TNF-α production in macrophages. To explore whether the altered cell wall of the *rim101*Δ mutant is able to differentially activate immune cells, we coincubated the WT and *rim101*Δ mutant strains with J774A macrophages and assessed TNF-α production after a short period of coincubation. The fungal cells were incubated overnight in tissue culture medium to induce capsule and cell wall changes and washed to minimize the effect of residual shed capsule on fungal-host cell interactions. When cocultured with macrophages for 4.5 h, the *rim101*Δ mutant strain induced significantly more TNF-α production than the WT strain (Fig. 6).

To address whether the shed capsular components from the different strains result in different host cell responses in this assay, we examined the production of TNF-α after incubating J774A.1 cells with conditioned medium from the WT or the *rim101*Δ mutant. Conditioned medium from either strain resulted in similar repression of TNF-α production by these macrophage-like cells, suggesting that the well-documented immunosuppressant properties of *C. neoformans* capsule are not compromised in the *rim101*Δ mutant strain (Fig. 6). Therefore, the altered cell surface of the *rim101*Δ mutant strain, and not its secreted exopolysaccharide, is likely the primary microbial feature resulting in accelerated activation of the host immune system.

DISCUSSION

The *rim101*Δ mutant strain causes a fundamentally different disease. Historically, treatment of infectious diseases has focused primarily on rapid eradication of the pathogen. However, antimicrobial agents are often insufficient to cure infections in the absence of an effective immune system. Moreover, an overexuberant host immune response can be equally detrimental to patient outcome. This balance of killing the pathogen and modulating the host immune response is exemplified in the practice of combining antibacterial therapy and corticosteroids to treat some types of bacterial meningitis (43).

Recently, IRIS has emerged as an important aspect of the clinical management of various infectious diseases. In patients with advanced AIDS, antiretroviral therapy (ART) can result in rapid restoration of the immune system. As viral replication is impaired, the patient's $CD4^+$ T cells can recover, resulting in various degrees of immune restoration. This immune reconstitution can lead to intense cell-mediated responses to latent or subclinical infections, leading to increased symptoms of disease despite effective clearance of the pathogen (44). Excessive IRIS in cryptococcal disease is associated with high morbidity and mortality. Various studies have reported that between 8 and 50% of AIDS patients develop cryptococcal IRIS after treatment with ART, even when previously treated with antifungal therapies, emphasizing the importance of this phenomenon in the management of cryptococcal meningitis (44, 45). In one study, the patients who developed IRIS had increased levels of several Th1 and innate cytokines in their CSF during the effector phase of the disease (45).

The excessive virulence of the *rim101*Δ mutant strain is likely due to aberrant stimulation of immune responses, similar to what is observed in cases of IRIS during infections with WT clinical strains. Generally, death of immunosuppressed patients from cryptococcosis is due to a combination of proliferation of cryptococcal cells within the brain and lungs of the host, as well as damage from the host immune response to these organisms. However,

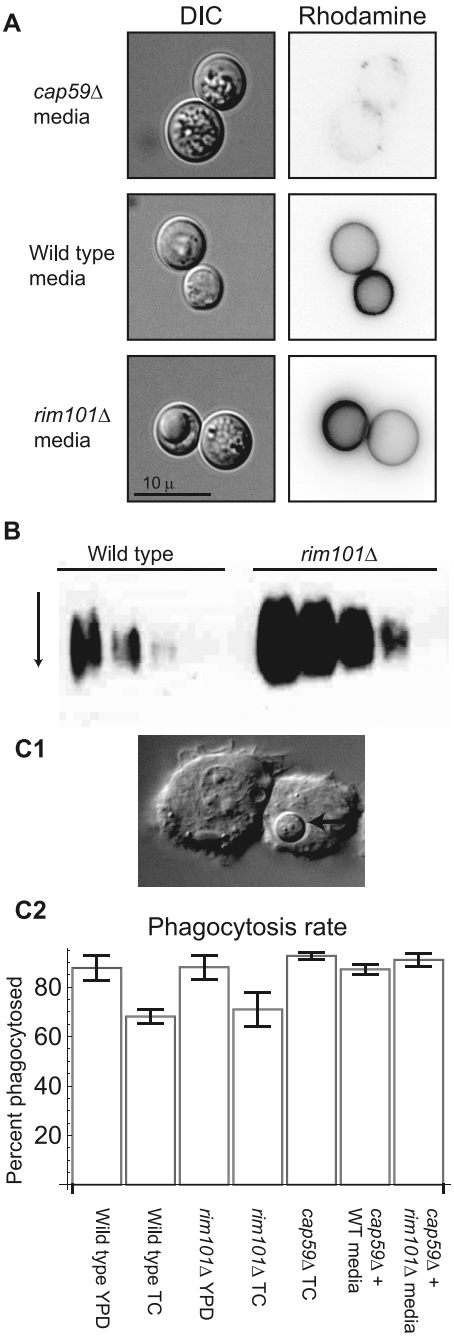

FIG 5 Rim101 regulates capsule attachment. (A) Secreted polysaccharide from *rim101*Δ mutant cells binds the cell surface similarly to that from WT cells. *cap59*Δ mutant cells were incubated with conditioned medium from the *cap59*Δ mutant, WT, or *rim101*Δ mutant strain. Secreted polysaccharide passively bound to the cell surface was visualized by using an anti-GXM antibody. DIC, differential interference contrast. (B) The *rim101*Δ mutant strain secretes more GXM than the WT. Equivalent cell numbers of the indicated strains were incubated in CO_2-independent capsule-inducing medium for 24 h before pelleting to remove the cells. The supernatant was then serially diluted (2-fold) and subjected to gel electrophoresis and immunoblotting with an anti-GXM antibody. (C1, C2) Phagocytosis is regulated by capsule and cell wall components. (C1) A representative phagocytosed cryptococcal cell. Arrows indicate the engulfed cell. (C2) Phagocytosis rates were measured after coincubation of J774A.1 cells and cryptococcal strains for 2 h. Unphagocytosed yeast cells were removed by gentle washing, and the phagocytic index was determined by quantitative culture. Student's *t* test was performed to determine statistically significant differences.

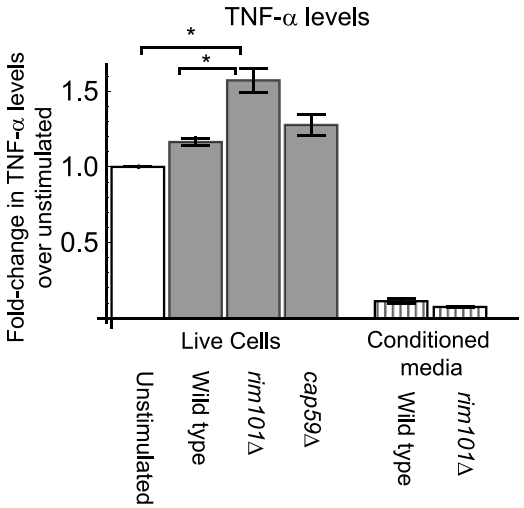

FIG 6 The *rim101*Δ mutant strain induces different TNF-α responses than the WT. Serum-starved macrophages (1×10^4) were coincubated with live WT, *rim101*Δ mutant, or *cap59*Δ mutant cells or with conditioned medium from the WT or *rim101*Δ mutant strain. After 4.5 h, TNF-α levels in the supernatants were measured by ELISA. Macrophages incubated without cryptococcal cells were used as the control. Student's *t* test was performed to determine statistically significant differences (*). Gray, response to live cells; vertical stripes, response to conditioned medium. The results are from three independent experiments. Unstimulated J774A.1 cells produced TNF-α at 82.66 ± 16.39 pg/ml.

we observed that mice infected with the *rim101*Δ mutant strain showed significantly decreased fungal burdens, despite demonstrating death kinetics similar to those of mice infected with the WT strain.

Histopathologic examination of *rim101*Δ mutant-infected mouse lungs demonstrated an increased influx of inflammatory cells, especially polymorphonuclear (PMN) cells and eosinophils, indicative of a fundamentally different nature of disease progression than infection with WT strains. Cytospin analysis confirmed the consistent increase in the percentage of PMN cells after infection with the *rim101*Δ mutant strain. Previous work on the role of neutrophils in cryptococcal disease revealed that, in contrast to many other fungal infections, early neutrophil influx into the infected lungs could be detrimental to the outcome of cryptococcal infections. Transient antibody-mediated inhibition of neutrophils at an early time point in *C. neoformans* infections resulted in increased survival of the mice (46). In another study, skewing the immune cell infiltrate toward a higher proportion of neutrophils (by removing dendritic cells and alveolar macrophages) also resulted in an increased death rate after infection with *C. neoformans* (47). Although resistant SJL/J mice have greater neutrophilia than susceptible C57BL/6 mice after infection with *C. neoformans*, the increased neutrophil levels were associated with more areas of localized inflammation (48). These studies are consistent with our results demonstrating that an early, aggressive innate immune response characterized by neutrophil influx into the lungs can cause disruption of the optimal balance between microbial clearance and host damage.

Additionally, the cytokine profile of the infected lungs confirmed that WT cells are very effective at actively preventing an excessive inflammatory response. We hypothesize that this process of immune evasion is mediated in part through the Rim101

protein. In *rim101*Δ mutant-infected lungs, we observed higher levels of a number of proinflammatory cytokines than in WT-infected lungs, including TNF-α, IP-10, MIG, MIP-1α, VEGF, and IL-12. In most cryptococcal infections, increased Th1 cytokine levels (TNF-α, IL-12, and IFN-γ) are associated with a decreased lung CFU count and an overall protective Th1 immune response (49–51). Interestingly, we observed an increase in TNF-α, IL-12, IP-10, and MIG levels without a corresponding increase in IFN-γ in *rim101*Δ mutant-infected mouse lungs at the particular time point used for these studies. Previous work has demonstrated that some of the protective effects of Th1 responses, including repression of eosinophil recruitment, are dependent on IFN-γ, potentially explaining the increased levels of eosinophils in *rim101*Δ mutant-infected mice (28, 52). Increased levels of MIG and IP-10 are often used as markers of allergic airway inflammation (53), and increased VEGF levels are also associated with pathological Th2 responses, especially in the context of asthma (54). However, we did not observe an increase in the Th2 cytokines (IL-4, IL-5, and IL-13) that are the major drivers of allergic airway inflammation, suggesting that the inflammation in the *rim101*Δ mutant-infected lungs was driven primarily by Th1-associated cytokines.

Lymphocytes were not a significant component of the inflammatory cell infiltration in either WT or *rim101*Δ mutant infections at these early time points, emphasizing the role of the innate immune system in responding to the exposed *rim101*Δ mutant cell wall.

Rim101 regulates remodeling of the cell wall upon entry into the host. To understand the mechanism by which the *rim101*Δ mutant strain provokes this aberrant immune response, we examined the host-pathogen interface, especially in the context of decreased capsule shielding by the *rim101*Δ mutant strain. Exposure of cell wall components, especially those that are conserved PAMPs, can stimulate the host immune response. Recent work with *C. albicans* has established a model in which the innate immune system responds to fungal pathogens, as reviewed in reference 55. In *C. albicans* and *Saccharomyces cerevisiae*, increased exposure of β-glucan is sufficient to induce the host inflammatory response via C-type lectin receptors on host cells (17, 19, 56, 57). Additionally, Cross and Bancroft demonstrated that, in acapsular strains of *C. neoformans*, mannose and β-glucan receptors on macrophages are important in binding to cryptococcal cells, and this binding results in increased phagocytosis and cytokine production (58).

We demonstrated that *C. neoformans* Rim101 activation plays a profound role in maintaining and remodeling the cell wall under host conditions. Our RNA sequencing experiments revealed that many cell wall genes were significantly differentially regulated in the *rim101*Δ mutant and the WT strain. Many of these genes had potential Rim101 binding sites in their putative promoter regions. In other fungi, Rim101 is also involved in the regulation and remodeling of cell walls, especially under host or stress conditions. In *S. cerevisiae*, Rim101 participates directly in cell wall assembly and remodeling by acting together with the protein kinase C signaling pathway (59). The yeast-hyphal transition, which is necessary for virulence in *C. albicans*, is dependent on CaRim101 (30, 32). Additionally, *C. albicans* uses Rim101 to regulate the expression of Phr1 and Phr2, which are β-glycosidases that are involved in cell wall remodeling (30).

We observed that the alterations in the *C. neoformans rim101*Δ mutant cell wall appear to be due mostly to excess chitin oligomers. Although the interactions between the host response and chitin are unclear, especially because of variable sources and processing, chitin has been linked with increased eosinophil recruitment and other allergic responses (60, 61). Interestingly, we also saw a significant increase in α-glucan levels in both strains after induction under host-mimicking conditions. These results are the first indication that α-glucan is induced upon entry into the host. Previous work on α-glucan in *C. neoformans* has demonstrated that this molecule is necessary for capsule attachment to the cell (39, 41). The induction of α-glucan in the WT strain is correlated with an increase in the capsule diameter around the cell. However, the *rim101*Δ mutant exhibited more α-glucan staining than the WT strain, consistent with the subtle increase in transcription of the α-glucan synthase gene in the *rim101*Δ mutant, despite the defect in capsule attachment. We hypothesize that this moiety is not sufficient to maintain the capsule at the cell surface. It is possible that the overall structure of the *rim101*Δ mutant cell wall is altered to such a degree that α-glucan cannot maintain the capsule. Further analysis of the *rim101*Δ mutant strain will provide more insight into the components and structures required for capsule attachment.

Additional complexity comes from the documented role of α-glucan in masking other, more immunogenic, molecules from the host. Work with *H. capsulatum* has demonstrated that α-glucan can mask highly immunostimulatory β-glucan from recognition by the dectin-1 receptor (18, 37). In *C. neoformans*, however, α-glucan may not act as an effective shield because the *rim101*Δ mutant strain stimulated more inflammation than the WT. Additionally, we did not observe significant IL-10 production in any of the infected lungs, suggesting that C-type lectins play a relatively minor role in the response to *C. neoformans* that we observed in this model (57), thus minimizing the effect of increased α-glucan shielding.

In addition to cell wall changes, alterations in capsule attachment and total levels of capsular polysaccharide may also partially explain the differential immune responses. At a systemic level, GXM has been used as a potent immunosuppressive and anti-inflammatory agent, ameliorating the effects of both collagen- and Group B Steptococcus-induced arthritis in rat models and lipopolysaccharide-induced sepsis in mice (62–65). Although the WT and the *rim101*Δ mutant synthesize similar levels of capsule (20), the increase in WT cells likely contributes to the increased levels of capsular polysaccharide in the host. This may be effective at damping the host immune response to WT cells. However, many infections using a wide range of inoculum doses of the WT strain have all failed to produce the type of inflammation triggered by the *rim101*Δ mutant strain. Additionally, completely acapsular strains, such as the *cap59*Δ mutant strain, also fail to cause this characteristic lung inflammation phenotype.

Another potential consequence of decreased capsule attachment in the *rim101*Δ mutant strain is the increased exposure of mannoproteins, which can then induce IL-12 production (66–68). Increased IL-12 can induce increased MIP-1α, which plays a role in the recruitment of leukocytes, especially macrophages and neutrophils (69).

Finally, titan cells, which are a recently described *C. neoformans* morphotype, are characterized by thickened cell walls and altered capsule attachment, in addition to massively increased cell size (22, 23). Titan cells inhibit phagocytosis, and the degree of inflam-

mation in the lungs is higher when the number of titan cells decreases (23). The *rim101*Δ mutant strain has a demonstrated defect in titan cell formation in our experiments and in previous observations (24). By histology, we observed that only 2.0% of *rim101*Δ mutant cells were titans, compared to 33.6% of the WT cells. The inability of the *rim101*Δ mutant to appropriately remodel cell walls under host conditions may be responsible for the lack of titan cell formation by this strain. Additionally, the dramatic reduction in the number of titan cells may also be a factor in the increased inflammatory response that we see in *rim101*Δ mutant infections. However, we were unable to completely abrogate the inflammation when adding WT cells as a source of titan cells to a *rim101*Δ mutant-infected mouse, implying that a decrease in titan cell formation is not sufficient to explain the *rim101*Δ mutant virulence phenotype. Together, these data suggest the hypothesis that CnRim101 directs remodeling of the cell wall when activated by host-specific stresses, thus minimizing the inflammatory immune response.

In summary, we previously demonstrated that *C. neoformans* responds to specific host signals by cleaving the Rim101 protein (20). Activated Rim101 induces cell wall changes that favor capsule attachment and minimize PAMP exposure. Both of these Rim101-mediated cell wall events have potentially important implications for pathogen survival in the host. Without Rim101, the cell is unable to mask immunogenic PAMPs, which could then trigger increased and aberrant inflammation in the mouse lung. *rim101*Δ mutant cells also have decreased survival in the harsh host environment, potentially reducing the overall levels of immunosuppressive GXM in the host organism. These studies therefore demonstrate fundamental ways in which pathogens induce protective phenotypes to avoid detection and actively modulate the host immune response, thus determining the outcome of the infectious process.

MATERIALS AND METHODS

Strains and medium. The *C. neoformans* strains used in this study were H99, a *rim101*Δ mutant (TOC2), a *rim101*Δ *RIM101* mutant (TOC4), a *cap59*Δ *rim101*Δ mutant (TOC39), and a *cap59*Δ mutant (5, 9, 20, 70). Capsule-inducing medium (DMEM with 25 mM $NaHCO_3$) was prepared as previously described (71).

Virulence and data analysis. The virulence of the *C. neoformans* strains was assessed by using a murine inhalation model of cryptococcosis, as described previously (72). Ten female C57BL/6 mice were inoculated intranasally with 2×10^4 *C. neoformans* cells of the WT, *rim101*Δ mutant, *cap59*Δ *rim101*Δ double mutant, or *cap59*Δ mutant strain. Mice were monitored daily for signs of infection and sacrificed at predetermined clinical endpoints predicting death. The statistical significance of differences between the survival curves of all of the animals infected with each strain was evaluated by using the log-rank test, and *P* values are reported in Results (JMP software; SAS Institute, Cary, NC). Cell counts were analyzed by using Student's unpaired *t* test. All studies were performed in compliance with institutional guidelines for animal experimentation.

For coinfections, two female A/J mice were inoculated intranasally with 5×10^5 cryptococcal cells at a 1:1, 2:1, or 1:2 ratio of WT to *rim101*Δ mutant cells. For irradiated-cell infections, two female A/J mice were inoculated intranasally with 5×10^5 UV-irradiated WT or *rim101*Δ mutant cells. Before irradiation, the cells were incubated overnight in DMEM with 5% CO_2 at 37°C to induce capsule formation. For cytokine analysis, 13 female A/J mice were inoculated intranasally with 5×10^5 WT or *rim101*Δ mutant cells in a 25-μl volume or with 25 μl of sterile PBS.

Histopathologic analysis. Lungs of A/J or C57BL/6 mice were inflated and harvested in 10% neutral buffered formalin at the indicated days postinfection. All lungs were then embedded in paraffin, cut into 5-μm-thick slices, and stained with H&E by the Duke histopathology core facility. All slides were examined by light microscopy.

Cytospin and cytokine preparations. The lungs of euthanized mice were lavaged twice with 0.5 ml of lavage buffer (PBS with EDTA) for cytokine collection (1-ml total volume) and a further 10 times (5-ml total volume) to obtain cells for cytospin analysis according to established protocols (48). The supernatant of the first milliliter of lavage fluid was used for multiplex cytokine analysis. The remaining cells were combined with cells from the last 5 ml and resuspended in a total volume of 1 ml. Cell densities were then normalized to 1×10^5/ml by hemacytometer, and 200 μl was centrifuged onto slides. Slides were stained with H&E and manually inspected to directly quantify the nature of the host cells in the lung cell infiltrate, as described previously (73). At least 300 cells were counted per sample. To quantify the immune cell infiltrate, cryptococcal CFU counts were subtracted from the normalized cell counts obtained by hemacytometer. Statistical significance was determined by performing one-way analysis of variance (ANOVA) with Bonferroni correction.

To determine cryptococcal cell diameters after infection, 0.5 ml of the lavage fluid was pelleted and resuspended in 0.05% SDS to lyse mammalian cells. The remaining cryptococcal cells were washed three times in water. Cells were obtained from at least three mice per strain. To determine *in vitro* cell diameters, all strains were incubated overnight in CO_2-independent medium at 37°C. All cell diameters were quantified by using ImageJ, and titan cells were defined as cells with a diameter greater than 15 μm (22). Capsules were not included in diameter measurements. At least 500 cells were counted for each sample.

Multiplex cytokine analysis. Fibroblast growth factor basic, granulocyte-macrophage colony-stimulating factor, IFN-γ, IL-1α, IL-1β, IL-2, IL-4, IL-5, IL-6, IL-10, IL-12, IL-13, IL-17, IP-10, KC, MCP-1, MIG, MIP-1α, TNF-α, and VEGF were analyzed using the Invitrogen Cytokine Mouse 20-Plex Panel on a Bio-Plex Luminex-100 machine at the Duke Human Vaccine Institute shared-resource facility in accordance with the manufacturer's instructions.

ELISA. J774A.1 macrophages (1×10^4/well) were inoculated into 96-well plates and incubated for 15 h in medium with 1% fetal bovine serum. Macrophages were then coincubated with 100 μl of either medium or cryptococcal cells (1×10^4 cells/well) for 4.5 h at 37°C with 5% CO_2. The supernatant was then removed, and TNF-α levels were assessed by enzyme-linked immunosorbent assay (ELISA) by following the manufacturer's instructions (Mouse TNF-α ELISA MAX standard kit; BioLegend, San Diego, CA).

Phagocytic index. To examine phagocytosis, we directly measured the interactions of macrophages according to previous protocols, with some modifications (11, 74). J774A.1 cells (1×10^5/well) were added to 96-well plates and activated by the addition of PMA and incubation for 2 h at 37°C with 5% CO_2. Then, 10^5 cryptococcal cells/well were added and the mixture was coincubated for 2 h. Unengulfed cells were removed by gentle washing with 2×50 μl PBS. The macrophages were then lysed with 100 μl of 0.5% SDS, and the phagocytosed cells were plated for CFU counting.

RNA preparation, sequencing, and transcript analysis. To induce expression changes, all strains were incubated in YPD to mid-log phase, washed twice, and then incubated in DMEM at 37°C with 5% CO_2 or YPD for 3 h. Cells were then washed twice, frozen on dry ice, and lyophilized for 3 h. Total RNA was extracted by using the Qiagen RNeasy Plant Minikit (Qiagen, Valencia, CA) as previously described (20).

Library preparation and RNA sequencing were performed by the Duke Sequencing Core Facility. Total RNA samples were purified and prepared according to the manufacturer's protocols (Illumina, San Diego, CA) and as previously described (24). Sequencing was performed on a GAII Illumina Genome Analyzer. To achieve sufficient sequence coverage for a reference transcriptome, the WT sample was sequenced with 72-bp paired-end reads. The *rim101*Δ mutant sample was sequenced with 36-bp single-end reads.

All reads were mapped to the *C. neoformans* reference genome pro-

vided by the Broad Institute by using TopHat v1.3.0 (75, 76). The aligned reads were then analyzed for the number of fragments per kilobase of transcript per million mapped reads by using Cufflinks v.1.0.3. Statistically significant differences between strains was determined by CuffDiff (77). Of the 2.3×10^7 reads for the WT sample, only 5.7×10^4 (0.2%) were filtered for poor quality. The *rim101*Δ mutant sample had less than 0.5% of the reads excluded. Genes were considered significantly differentially expressed if *P* values were greater than the false-discovery rate after Benjamini-Hochberg corrections for multiple testing and if the change was greater than 2.0-fold.

RNA was converted to cDNA with the Clontech Advantage RT for PCR kit according to the manufacturer's instructions. Semiquantitative RT-PCR was performed, and the *n*-fold change was determined by ImageJ analysis of the resulting amplicons. All of the primers used for RT-PCR assays are listed in Table S4 in the supplemental material.

Electron microscopy. Electron microscopy was performed at the Center for Electron Microscopy at North Carolina State University. Cells were incubated at 37°C in DMEM with 5% CO_2 until they reached log-phase growth. Cells were fixed according to the procedures developed by Reese et al. (41).

Cell wall analysis. For cell wall staining, strains were washed and then stained with either 0.01% aniline blue (β-glucan) or WGA conjugated to Alexa Fluor 488 (chitin) (Molecular Probes, Eugene, OR) (35, 38). After staining, cells were washed twice before observation by fluorescence microscopy. Aniline blue staining was observed by using a 350-nm wavelength for fluorescence, and WGA was observed by using a 488-nm wavelength for fluorescence. To visualize α-glucan, cells were incubated with the α-(1,3)-glucan MOPC-104E antibody (Sigma, St. Louis, MO) and a fluorescent IgM anti-mouse antibody (Sigma) as previously described (37). Fluorescence was measured at a 494-nm wavelength. Bright-field, differential interference contrast, and fluorescence microscopy images were captured with a Zeiss Axio Imager.A1 fluorescence microscope equipped with an AxioCam MRm digital camera.

Chitin/chitosan levels were determined according to the method developed by Lehmann and White (34), by using 20 U of optical density at 600 nm per strain to normalize the number of cells for each sample.

Capsule quantification assays. Conditioned medium was made by incubating cells in CO_2-independent medium (Gibco) for 24 h. This tissue culture medium results in capsule induction, similar to DMEM. Unlike previous experiments where the cells were heated at 70°C to release the capsule, these cells were left untreated. To collect the conditioned medium, a 1-ml culture sample was centrifuged at 14,000 rpm to remove cells. The supernatant from each medium sample was used to prepare a series of 2-fold dilutions, and 10 μl of each dilution was subjected to gel electrophoresis and immunoblotting as previously described (20, 39).

Capsule attachment assays. Capsule attachment was performed by incubating *cap59*Δ mutant cells with conditioned medium as previously described (39). The capsule was visualized by using anti-GXM MAb 18b7 and an Alexa Fluor 594-conjugated anti-mouse secondary antibody (Invitrogen).

Nucleotide sequence accession number. All of the nucleotide sequence data obtained were uploaded to the NCBI GEO database under accession number GSE43189.

SUPPLEMENTAL MATERIAL

Supplemental material for this article may be found at http://mbio.asm.org/lookup/suppl/doi:10.1128/mBio.00522-12/-/DCSupplemental.

Figure S1, EPS file, 2.3 MB.
Table S1, DOCX file, 0.1 MB.
Table S2, DOCX file, 0.1 MB.
Table S3, XLSX file, 0.1 MB.
Table S4, XLSX file, 0.1 MB.

ACKNOWLEDGMENTS

We thank the Duke Sequencing Core Facility, the Duke Human Vaccine Institute Biomarker Analysis shared-resource facility, the North Carolina State University electron microscopy facility, and the Duke histopathology core facility for their assistance. We thank Arturo Casadevall for MAb 18b7. We thank Gregory D. Sempowski for consultation on multiplex assays and critical reading of the manuscript.

These studies were supported by NIH grants AI050128 and AI074677 (J.A.A.) and an American Heart Association predoctoral fellowship (T.R.O.).

REFERENCES

1. **Park BJ, et al.** 2009. Estimation of the current global burden of cryptococcal meningitis among persons living with HIV/AIDS. AIDS **23**:525–530.
2. **Chau TA, et al.** 2009. Toll-like receptor 2 ligands on the staphylococcal cell wall downregulate superantigen-induced T cell activation and prevent toxic shock syndrome. Nat. Med. **15**:641–648.
3. **Diamond RD, Bennett JE.** 1974. Prognostic factors in cryptococcal meningitis: a study in 111 cases. Ann. Intern. Med. **80**:176–181.
4. **Singh N, Perfect JR.** 2007. Immune reconstitution syndrome associated with opportunistic mycoses. Lancet Infect. Dis. **7**:395–401.
5. **Chang YC, Kwon-Chung KJ.** 1994. Complementation of a capsule-deficient mutation of *Cryptococcus neoformans* restores its virulence. Mol. Cell. Biol. **14**:4912–4919.
6. **Chang YC, Penoyer LA, Kwon-Chung KJ.** 1996. The second capsule gene of *Cryptococcus neoformans*, CAP64, is essential for virulence. Infect. Immun. **64**:1977–1983.
7. **Chang YC, Kwon-Chung KJ.** 1998. Isolation of the third capsule-associated gene, CAP60, required for virulence in *Cryptococcus neoformans*. Infect. Immun. **66**:2230–2236.
8. **Kozel TR, Cazin J, Jr.** 1971. Nonencapsulated variant of *Cryptococcus neoformans*. I. Virulence studies and characterization of soluble polysaccharide. Infect. Immun. **3**:287–294.
9. **D'Souza CA, et al.** 2001. Cyclic AMP-dependent protein kinase controls virulence of the fungal pathogen *Cryptococcus neoformans*. Mol. Cell. Biol. **21**:3179–3191.
10. **Mylonakis E, Ausubel FM, Perfect JR, Heitman J, Calderwood SB.** 2002. Killing of *Caenorhabditis elegans* by *Cryptococcus neoformans* as a model of yeast pathogenesis. Proc. Natl. Acad. Sci. U. S. A. **99**:15675–15680.
11. **Feldmesser M, Kress Y, Novikoff P, Casadevall A.** 2000. *Cryptococcus neoformans* is a facultative intracellular pathogen in murine pulmonary infection. Infect. Immun. **68**:4225–4237.
12. **Vecchiarelli A, et al.** 2003. The polysaccharide capsule of *Cryptococcus neoformans* interferes with human dendritic cell maturation and activation. J. Leukoc. Biol. **74**:370–378.
13. **Kozel TR, Gotschlich EC.** 1982. The capsule of *Cryptococcus neoformans* passively inhibits phagocytosis of the yeast by macrophages. J. Immunol. **129**:1675–1680.
14. **Zaragoza O, et al.** 2008. Capsule enlargement in *Cryptococcus neoformans* confers resistance to oxidative stress suggesting a mechanism for intracellular survival. Cell. Microbiol. **10**:2043–2057.
15. **Gates MA, Kozel TR.** 2006. Differential localization of complement component 3 within the capsular matrix of *Cryptococcus neoformans*. Infect. Immun. **74**:3096–3106.
16. **Zaragoza O, Taborda CP, Casadevall A.** 2003. The efficacy of complement-mediated phagocytosis of *Cryptococcus neoformans* is dependent on the location of C3 in the polysaccharide capsule and involves both direct and indirect C3-mediated interactions. Eur. J. Immunol. **33**:1957–1967.
17. **Netea MG, et al.** 2006. Immune sensing of *Candida albicans* requires cooperative recognition of mannans and glucans by lectin and Toll-like receptors. J. Clin. Invest. **116**:1642–1650.
18. **Rappleye CA, Goldman WE.** 2008. Fungal stealth technology. Trends Immunol. **29**:18–24.
19. **Wheeler RT, Kupiec M, Magnelli P, Abeijon C, Fink GR.** 2003. A Saccharomyces cerevisiae mutant with increased virulence. Proc. Natl. Acad. Sci. U. S. A. **100**:2766–2770.
20. **O'Meara TR, et al.** 2010. Interaction of *Cryptococcus neoformans* Rim101 and protein kinase A regulates capsule. PLoS Pathog. **6**:e1000776.
21. **Liu OW, et al.** 2008. Systematic genetic analysis of virulence in the human fungal pathogen *Cryptococcus neoformans*. Cell **135**:174–188.
22. **Okagaki LH, et al.** 2010. Cryptococcal cell morphology affects host cell interactions and pathogenicity. PLoS Pathog. **6**:e1000953.

23. **Zaragoza O, et al.** 2010. Fungal cell gigantism during mammalian infection. PLoS Pathog. **6**:e1000945.
24. **Okagaki LH, et al.** 2011. Cryptococcal titan cell formation is regulated by G-protein signaling in response to multiple stimuli. Eukaryot. Cell **10**: 1306–1316.
25. **Okagaki LH, Nielsen K.** 2012. Titan cells confer protection from phagocytosis in *Cryptococcus neoformans* infections. Eukaryot. Cell **11**:820–826.
26. **Giles SS, Zaas AK, Reidy MF, Perfect JR, Wright JR.** 2007. Cryptococcus neoformans is resistant to surfactant protein A mediated host defense mechanisms. PLoS One **2**:e1370.
27. **Kawakami K, et al.** 1999. Chemokine responses and accumulation of inflammatory cells in the lungs of mice infected with highly virulent *Cryptococcus neoformans*: effects of interleukin-12. FEMS Immunol. Med. Microbiol. **25**:391–402.
28. **Kawakmami K, et al.** 1999. Interferon-gamma (IFN-γ)-dependent protection and synthesis of chemoattractants for mononuclear leucocytes caused by IL-12 in the lungs of mice infected with *Cryptococcus neoformans*. Clin. Exp. Immunol. **117**:113–122.
29. **Olszewski MA, et al.** 2000. The role of macrophage inflammatory protein-1 alpha/CCL3 in regulation of T cell-mediated immunity to *Cryptococcus neoformans* infection. J. Immunol. **165**:6429–6436.
30. **Davis DA.** 2009. How human pathogenic fungi sense and adapt to pH: the link to virulence. Curr. Opin. Microbiol. **12**:365–370.
31. **Liu H.** 2001. Transcriptional control of dimorphism in *Candida albicans*. Curr. Opin. Microbiol. **4**:728–735.
32. **Nobile CJ, et al.** 2008. Candida albicans transcription factor Rim101 mediates pathogenic interactions through cell wall functions. Cell. Microbiol. **10**:2180–2196.
33. **Baek YU, Martin SJ, Davis DA.** 2006. Evidence for novel pH-dependent regulation of *Candida albicans* Rim101, a direct transcriptional repressor of the cell wall beta-glycosidase Phr2. Eukaryot. Cell **5**:1550–1559.
34. **Lehmann PF, White LO.** 1975. Chitin assay used to demonstrate renal localization and cortisone-enhanced growth of *Aspergillus fumigatus* mycelium in mice. Infect. Immun. **12**:987–992.
35. **Fox DS, Cox GM, Heitman J.** 2003. Phospholipid-binding protein Cts1 controls septation and functions coordinately with calcineurin in *Cryptococcus neoformans*. Eukaryot. Cell **2**:1025–1035.
36. **Rodrigues ML, Alvarez M, Fonseca FL, Casadevall A.** 2008. Binding of the wheat germ lectin to *Cryptococcus neoformans* suggests an association of chitinlike structures with yeast budding and capsular glucuronoxylomannan. Eukaryot. Cell **7**:602–609.
37. **Rappleye CA, Eissenberg LG, Goldman WE.** 2007. Histoplasma capsulatum a-(1,3)-glucan blocks innate immune recognition by the b-glucan receptor. Proc. Natl. Acad. Sci. U. S. A. **104**:1366–1370.
38. **Shedletzky E, Unger C, Delmer DP.** 1997. A microtiter-based fluorescence assay for (1,3)-beta-glucan synthases. Anal. Biochem. **249**:88–93.
39. **Reese AJ, Doering TL.** 2003. Cell wall alpha1,3-glucan is required to anchor the *Cryptococcus neoformans* capsule. Mol. Microbiol. **50**: 1401–1409.
40. **Garcia-Rivera J, Chang YC, Kwon-Chung KJ, Casadevall A.** 2004. Cryptococcus. *neoformans* CAP59 (or Cap59p) is involved in the extracellular trafficking of capsular glucuronoxylomannan. Eukaryot. Cell **3**:385–392.
41. **Reese AJ, et al.** 2007. Loss of cell wall alpha(1–3) glucan affects *Cryptococcus neoformans* from ultrastructure to virulence. Mol. Microbiol. **63**: 1385–1398.
42. **Chun CD, Madhani HD.** 2010. Ctr2 links copper homeostasis to polysaccharide capsule formation and phagocytosis inhibition in the human fungal pathogen *Cryptococcus neoformans*. PLoS One **5**:e12503.
43. **van de Beek D, de Gans J, McIntyre P, Prasad K.** 2004. Steroids in adults with acute bacterial meningitis: a systematic review. Lancet Infect. Dis. **4**:139–143.
44. **Shelburne SA, et al.** 2005. The role of immune reconstitution inflammatory syndrome in AIDS-related *Cryptococcus neoformans* disease in the era of highly active antiretroviral therapy. Clin. Infect. Dis. **40**:1049–1052.
45. **Boulware DR, et al.** 2010. Clinical features and serum biomarkers in HIV immune reconstitution inflammatory syndrome after cryptococcal meningitis: a prospective cohort study. PLoS Med. **7**:e1000384.
46. **Mednick AJ, Feldmesser M, Rivera J, Casadevall A.** 2003. Neutropenia alters lung cytokine production in mice and reduces their susceptibility to pulmonary *cryptococcosis*. Eur. J. Immunol. **33**:1744–1753.
47. **Osterholzer JJ, et al.** 2009. Role of dendritic cells and alveolar macrophages in regulating early host defense against pulmonary infection with *Cryptococcus neoformans*. Infect. Immun. **77**:3749–3758.
48. **Guillot L, Carroll SF, Homer R, Qureshi ST.** 2008. Enhanced innate immune responsiveness to pulmonary *Cryptococcus neoformans* infection is associated with resistance to progressive infection. Infect. Immun. **76**: 4745–4756.
49. **Milam JE, et al.** 2007. Modulation of the pulmonary type 2 T-cell response to *Cryptococcus neoformans* by intratracheal delivery of a tumor necrosis factor alpha-expressing adenoviral vector. Infect. Immun. **75**: 4951–4958.
50. **Jain AV, et al.** 2009. Th2 but not Th1 immune bias results in altered lung functions in a murine model of pulmonary *Cryptococcus neoformans* infection. Infect. Immun. **77**:5389–5399.
51. **Decken K, et al.** 1998. Interleukin-12 is essential for a protective Th1 response in mice infected with *Cryptococcus neoformans*. Infect. Immun. **66**:4994–5000.
52. **Cohn L, Homer RJ, Niu N, Bottomly K.** 1999. T helper 1 cells and interferon gamma regulate allergic airway inflammation and mucus production. J. Exp. Med. **190**:1309–1318.
53. **Fulkerson PC, et al.** 2004. Negative regulation of eosinophil recruitment to the lung by the chemokine monokine induced by IFN-gamma (Mig, CXCL9). Proc. Natl. Acad. Sci. U. S. A. **101**:1987–1992.
54. **Lee CG, et al.** 2004. Vascular endothelial growth factor (VEGF) induces remodeling and enhances TH2-mediated sensitization and inflammation in the lung. Nat. Med. **10**:1095–1103.
55. **Netea MG, Brown GD, Kullberg BJ, Gow NA.** 2008. An integrated model of the recognition of Candida albicans by the innate immune system. Nat. Rev. Microbiol. **6**:67–78.
56. **Wheeler RT, Fink GR.** 2006. A drug-sensitive genetic network masks fungi from the immune system. PLoS Pathog. **2**:e35.
57. **Geijtenbeek TB, Gringhuis SI.** 2009. Signalling through C-type lectin receptors: shaping immune responses. Nat. Rev. Immunol. **9**:465–479.
58. **Cross CE, Bancroft GJ.** 1995. Ingestion of acapsular *Cryptococcus neoformans* occurs via mannose and beta-glucan receptors, resulting in cytokine production and increased phagocytosis of the encapsulated form. Infect. Immun. **63**:2604–2611.
59. **Castrejon F, Gomez A, Sanz M, Duran A, Roncero C.** 2006. The RIM101 pathway contributes to yeast cell wall assembly and its function becomes essential in the absence of mitogen-activated protein kinase Slt2p. Eukaryot. Cell **5**:507–517.
60. **Reese TA, et al.** 2007. Chitin induces accumulation in tissue of innate immune cells associated with allergy. Nature **447**:92–96.
61. **Lenardon MD, Munro CA, Gow NA.** 2010. Chitin synthesis and fungal pathogenesis. Curr. Opin. Microbiol. **13**:416–423.
62. **Piccioni M, et al.** 22 October 2012. A purified capsular polysaccharide markedly inhibits inflammatory response during endotoxic shock. Infect. Immun.. [Epub ahead of print.] http://dx.doi.org/10.1128/IAI.00553-12.
63. **Monari C, et al.** 2009. A microbial polysaccharide reduces the severity of rheumatoid arthritis by influencing Th17 differentiation and proinflammatory cytokines production. J. Immunol. **183**:191–200.
64. **Mirshafiey A, et al.** 2004. Tolerability and anti-inflammatory effects of glucuronoxylomannan in collagen-induced arthritis. Scand. J. Immunol. **60**:226–232.
65. **Tissi L, et al.** 2004. Glucuronoxylomannan, the major capsular polysaccharide of *Cryptococcus neoformans*, inhibits the progression of group B streptococcal arthritis. Infect. Immun. **72**:6367–6372.
66. **Pitzurra L, et al.** 2000. Early induction of interleukin-12 by human monocytes exposed to *Cryptococcus neoformans* mannoproteins. Infect. Immun. **68**:558–563.
67. **Huang C, Nong SH, Mansour MK, Specht CA, Levitz SM.** 2002. Purification and characterization of a second immunoreactive mannoprotein from *Cryptococcus neoformans* that stimulates T-cell responses. Infect. Immun. **70**:5485–5493.
68. **Levitz SM, Nong SH, Mansour MK, Huang C, Specht CA.** 2001. Molecular characterization of a mannoprotein with homology to chitin deacetylases that stimulates T cell responses to *Cryptococcus neoformans*. Proc. Natl. Acad. Sci. U. S. A. **98**:10422–10427.
69. **Huffnagle GB, et al.** 1997. Macrophage inflammatory protein-1alpha (MIP-1alpha) is required for the efferent phase of pulmonary cell-mediated immunity to a *Cryptococcus neoformans* infection. J. Immunol. **159**:318–327.
70. **Perfect JR, Lang SD, Durack DT.** 1980. Chronic cryptococcal meningitis: a new experimental model in rabbits. Am. J. Pathol. **101**:177–194.

71. **Granger DL, Perfect JR, Durack DT.** 1985. Virulence of *Cryptococcus neoformans*. Regulation of capsule synthesis by carbon dioxide. J. Clin. Invest. **76**:508–516.
72. **Cox GM, Mukherjee J, Cole GT, Casadevall A, Perfect JR.** 2000. Urease as a virulence factor in experimental cryptococcosis. Infect. Immun. **68**: 443–448.
73. **Osterholzer JJ, et al.** 2009. Cryptococcal urease promotes the accumulation of immature dendritic cells and a non-protective T2 immune response within the lung. Am. J. Pathol. **174**:932–943.
74. **O'Meara TR, Hay C, Price MS, Giles S, Alspaugh JA.** 2010. *Cryptococcus neoformans* histone acetyltransferase Gcn5 regulates fungal adaptation to the host. Eukaryot. Cell **9**:1193–1202.
75. **Kovoor JM, et al.** 2002. Cryptococcal choroid plexitis as a mass lesion: MR imaging and histopathologic correlation. AJNR Am. J. Neuroradiol. **23**:273–276.
76. **Trapnell C, Pachter L, Salzberg SL.** 2009. Tophat: discovering splice junctions with RNA-Seq. Bioinformatics **25**:1105–1111.
77. **Trapnell C, et al.** 2010. Transcript assembly and quantification by RNA-Seq reveals unannotated transcripts and isoform switching during cell differentiation. Nat. Biotechnol. **28**:511–515.